Imaging of continuum states of the He$_2^{2+}$ quasimolecule

L. Ph. H. Schmidt,* M. S. Schöffler, K. E. Stiebing, H. Schmidt-Böcking, and R. Dörner

*Institut für Kernphysik, J. W. Goethe-Universität Frankfurt, Max-von-Laue-Straße 1, 60438 Frankfurt am Main,
Federal Republic of Germany*

F. Afaneh

Physics Department, The Hashemite University, P.O. Box 150459, Zarqa 13115, Jordan

Th. Weber

Lawrence Berkeley National Laboratory, Chemical Sciences Division, One Cyclotron Road, Berkeley, California 94720, USA
(Received 13 April 2007; published 3 July 2007)

Using cold target recoil ion momentum spectroscopy (COLTRIMS) we have investigated the production of one free electron in slow He^{2+}+He(1s^2) collisions. At projectile velocities between 0.6 and 1.06 a.u. (9–28 keV/u), the fully differential cross section was measured state selective with respect to the second electron, which is bound either at the target or the projectile. We provide a comprehensive data set comprising state selective total cross section, scattering angle dependent single differential cross sections, and fully differential cross section. We show that the momentum distribution of the electron in the continuum image the relevant molecular orbitals for the reaction channel under consideration. By choosing the bound electron final state at the target or projectile and the impact parameter we can select these orbitals and manipulate their relative phase.

I. INTRODUCTION

Charge transfer and simultaneous ionization reactions at slow He^{2+}+He collisions are time-dependent processes involving four strongly interacting particles. They are showcase examples for few body quantum dynamics in a regime where perturbation theory fails.

In these slow collisions the trajectories of the nuclei depend only slightly on the exact evolution of the electronic wave function. Therefore, it is possible to separate the equations of motion of the nuclei from those of the electrons. Reasonable results can be achieved using a semiclassical approximation at which the two nuclei move on classical trajectories. They establish the time-dependent two center potential which governs the evolution of the electronic wave function. To understand this dynamics it is suggestive to expand the electronic wave function in a time dependent basis, which consists of approximative solution of the adiabatic electronic Hamiltonian, i.e., molecular orbitals for this two center potential. The dynamics of the system is then considered by couplings between these molecular basis states and phase shifts. At projectile velocities below 1 a.u. a very small number of molecular basis states is sufficient for such a coupled channel calculation. For example, double electron capture [He^{2+}+He(1s^2)→He(1s^2)+He^{2+}] can be reasonably described by using only three basis states [1]. In the more recent work of Gao *et al.* [2] a fully quantum-mechanical molecular-orbital treatment was used yielding almost perfect agreement between theory and experiment.

Despite of the success of the close coupling method in describing electron transfer between bound states, the popu-

lation of continuum states was not sufficiently considered so far. This is in striking contrast to the importance of electron emission. At projectile velocities between 0.6 and 1 a.u., the total cross section of free electron production is approximately 20% of the single electron capture (SC) to the ground state SC1 [He^{2+}+He(1s^2)→He$^+$(1s)+He$^+$(1s)].

A very intuitive view of the ionization dynamics in slow collisions, termed saddle point mechanism (SP) was suggested by Olson based on purely classical considerations. In classical-trajectory Monte Carlo (CTMC) calculations [3–5] he found electrons emitted in forward direction with nearly half of the projectile velocity. He argued that *these electrons are ones that are left stranded equidistant between the projectile and target nucleus ions and are balanced in place by the attractive Coulomb forces of both ions* [6]. In the late 1980s several measurements at collision energies between 50 and 100 keV/u done at Rolla [7,8] and Bariloche [9–11] searched for the pronounced nuclear charge dependency of the electron emission pattern trying to demonstrate the existence of the SP mechanism. These experiments done with dispersive electron spectrometers yielded conflicting results. Only the Rolla group claimed evidence of the SP mechanism from their data.

An experimental breakthrough in this discussion was achieved by introducing electron time-of-flight measurements [12] and later electron imaging. A sequence of experiments showed that indeed in slow ion atom collisions the majority of the ejected electrons reside in between the target and the projectile in velocity space [13–22]. Whether the saddle point mechanism is responsible for this fact however remained a matter of controversy [23–25].

To describe the SP mechanism quantum mechanically within the molecular orbital (MO) approach, an infinite number of excited and continuum states would have to be con-

*Electronic address: Schmidt@atom.uni-frankfurt.de

TABLE I. Reaction channels in $He^{2+}+He$ collisions measured in this work.

Name of the process		Final state			
		Ejectile		Recoil ion	
Transfer ionization	TI	He^+	$+e^-$	$+He^{2+}$	
	TI1	$He^+(1s)$	$+e^-$	$+He^{2+}$	
	TI2	$He^+(nl)$	$+e^-$	$+He^{2+}$	$n \geq 2$
Single ionization	SI	He^{2+}	$+e^-$	$+He^+$	
	SI1	He^{2+}	$+e^-$	$+He^+(1s)$	
	SI2	He^{2+}	$+e^-$	$+He^+(nl)$	$n \geq 2$
Single capture	SC	He^+		$+He^+$	
	SC1	$He^+(1s)$		$+He^+(1s)$	
	SC2	$He^+(1s)$ or $He^+(2l)$		$+He^+(2l)$ or $+He^+(1s)$	
	SC3	$He^+(1s)$ or $He^+(nl)$		$+He^+(nl)$ or $+He^+(1s)$	$n \geq 3$
Double capture	DC	He^{2+}		$+He$	
	DC1	He^{2+}		$+He(1s^2)$	
	DC2	He^{2+}		$+He(1s,nl)$	$n \geq 2$
Autoionizing double capture	ADC	$He^{2+}+He^*$	$\rightarrow$	$He^{2+}+e^-+He^+(1s)$	

sidered, which is not feasible. A widely used workaround is to calculate within the MO approach, the population probability of molecular Rydberg states instead of the continuum. This has been done successfully in the hidden crossing theory [26]. While for the ionization in $p+H$ collisions analytical expressions for the eigenvalues of molecular states are available, the strength of the radial coupling can be estimated by integrating in the plane of complex inter nuclear distances [27,28]. In the correlation diagram adiabatic molecular states of the same symmetry approach but do not cross. At the internuclear distances of these so-called hidden crossings there is a strong radial coupling promoting the electron to the next higher MO. The continuum can finally be reached through an infinite number of hidden crossings at successively increasing internuclear distance.

More complex quantum-mechanical calculations of the ionization have been done using the two-center momentum-space discretization method [29,30] or by solving the emitted electron wave function at a lattice [31,32], but as the hidden crossing theory these calculations are limited to one active electron.

The increase of the couplings during the hidden crossing promotion indicates that weakly bound MOs are not practical for a detailed description of the system. Therefore Ovchinnikov and Macek [33] transformed the MOs to new, scaled coordinates. They demonstrated that different channels of hidden crossing promotion lead specifically to electron emission pattern, which reflect the symmetry of MOs populated at small internuclear distances by rotational coupling. The MOs of a two-electron system cannot be calculated analytically therefore the theory of Ovchinnikov and Macek cannot be adapted to He^{2+} on He collisions. Nevertheless, the findings of this theory can be used to guide the interpretation of the data presented in this work. We will use these arguments and show that the measured structure of the continuum elec-

tron momentum distribution unveils the bound MOs relevant for the promotion and that these can be manipulated by selecting impact parameters or states of the second, bound electrons.

In the following we present fully differential cross sections for single electron emission in He^{2+} on He collisions. This collision system generates the homonuclear He_2^{2+} quasimolecule which has a similar symmetry as H_2. The two electrons of the system are initially in a well-known state. To investigate the impact of electron correlation during the ionization process, we will analyze the electron emission pattern separately for four different final states of the second electron, which remains bound at one of the nuclei. At projectile velocity between 0.63 a.u. and 1.06 a.u. we have measured the single ionization (SI)

$$He^{2+} + He(1s^2) \rightarrow He^{2+} + e^- + He^+(nl), \qquad (1)$$

in which one electron remains at a bound state at the target as well as the transfer ionization (TI)

$$He^{2+} + He(1s^2) \rightarrow He^+(nl) + e^- + He^{2+}, \qquad (2)$$

which transfers one electron to the projectile. Each of these two reactions can be split up by separating different electron binding energies of the $He^+(nl)$. If the bound electron was found in ground state $(n=1)$ we denote the channels by SI1 and TI1, respectively. At SI2 and TI2 the bound electron is excited $(n \geq 2)$: see Table I.

II. EXPERIMENTAL SETUP

The experiment was conducted at the electron cycoltron resonance (ECR) ion source at the Institut für Kernphysik of the University Frankfurt (Main), Germany. The experimental setup has been described in more detail in [22,34], so only a

brief outline will be given here. Cold target recoil ion momentum spectroscopy (COLTRIMS) [35–37] was used to determine all three components of the ionized target momentum vector and its charge state. Three position sensitive multichannel plate detectors (MCP) with delay line readout [38] were used to detect the electron, the projectile, and the recoil ion. The recoil ion arm of the spectrometer was build in a time and position focusing geometry [39,40] to eliminate the deteriorating influence of spatial extension of the reaction volume on the momentum resolution. For a typical spectrometer field between 0.4 and 0.8 V/mm the momentum resolution was 0.2 a.u. in beam direction and 0.4 a.u. [full width of half maximum (FWHM)] transverse to the projectile beam.

The spectrometer generates a homogeneous electric field at the reaction volume, which projects the electron onto a second position sensitive MCP detector opposite to the recoil ion detector. The electron arm of the spectrometer had a total length of 40 mm, including a drift region. Drift and field region in Wiley-McLaren geometry [41] were separated by a grid. For each projectile velocity v_p the spectrometer voltage was adjusted so that electrons emitted with v_p in direction of the beam are detected close to the front edge of the detector. Thereby at the detector the velocity space between 0 and v_p was spread over approximately 55 mm.

The projectile beam was pulsed in bunches of 2 ns length with a repetition rate of 4 MHz to determine the reaction time and thereby to obtain the absolute time of flight of the electron as well as the recoil-ion within the spectrometer. For reaction channels where at least one electron was transferred the projectile was separated from the main beam by electrostatic deflection. These He⁺ and He projectiles were detected by a third position sensitive MCP detector to determine their charge state and to obtain a rough information about the scattering angle. Furthermore, this detector provided a more precise timing information (1 ns FWHM) than the beam pulser.

For pulsed beam measurements the electron velocity resolution at the plane of the detector (FWHM) was 0.08 times the projectile velocity v_p and 0.17 v_p in the perpendicular dimension.

Even though the scattering angle was measured by the projectile detector, the final state projectile momentum was calculated from electron and recoil ion momentum by using momentum conservation. Because the kinematically complete information was available the final state energy of the bound electron could be calculated using energy conservation. An energy resolution of 10 eV (FWHM) was achieved, which is sufficient to separate He⁺(1s) from excited states. This enables us to distinguish between transfer ionization into ground state TI1 and into excited states TI2, as well as between SI1 and SI2.

This separation of the electron emission into four channels and the simultaneous measurement of all these channels allow to investigate the effects of electron correlation during the collision. Earlier experiments on He²⁺+He collision [15,16], and other collision systems [14,17,18] had not measured the electron time of flight and therefore not obtained the kinematical complete information as well as the final state binding energy.
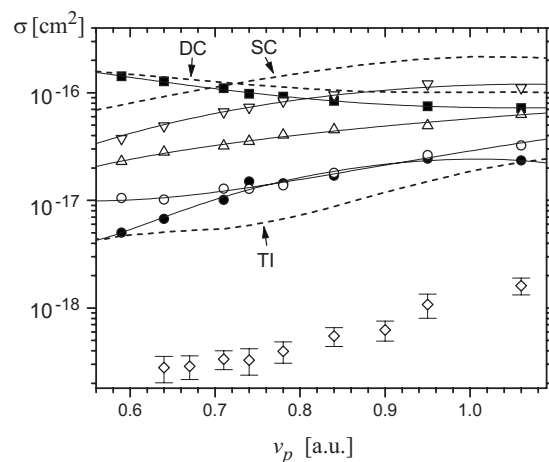

FIG. 1. Total cross sections of single and double capture into different electronic states: SC1 [He(1s)⁺+He(1s)⁺, open triangle], SC2 [He(1s)⁺+He(2l)⁺ and He(2l)⁺+He(1s)⁺, open inverted triangle], SC3 [He(1s)⁺+He(3l)⁺ and He(3l)⁺+He(1s)⁺, open circles], DC1 [He(1s²)+He²⁺, full squares], DC2 [He(1s,2l)+He²⁺, full circles], TI2 [He(2l)⁺+e⁻+He²⁺, open diamonds] the solid lines are drawn to guide the eye. Our data have been normalized to experimental results of Afrosimov *et al.* [42] (dashed lines).

III. RESULTS AND DISCUSSION

A. Total cross sections

Since our detection system covers 4π collection solid angle for the complete relevant final momentum space of all particles we can obtain ratios of total cross sections for the different reaction channels by integrating over momentum space. We took great care that our detection efficiency for charged particles did not depend on the charge state.

The measured momenta allow us to determine the final state binding energy of the target and projectile. This applies for TI and SI as well as the pure capture channels. With our energy resolution we can separate the single electron capture (SC), He²⁺+He→He⁺+He⁺ into three channels. SC1 is defined as the channel with both He⁺ at ground state. If either the projectile or the recoil ion is excited into the *L* shell we term the reaction SC2. At SC3 one electron is at the *M* shell or even higher excited while the second electron is still at ground state. For the double electron capture (DC) He²⁺ +He→He+He²⁺ we can separate the transfer into ground state (DC1) from transfer into excited states (DC2) with excitation energies of about 20 eV.

The density of our supersonic gas target is only approximately known. Therefore we normalized our data to the experimental total cross sections for DC and SC of Afrosimov *et al.* [42] and DuBois [43].

Figure 1 shows the total cross section as a function of the projectile velocity v_p. At the highest v_p of 1.06 a.u. the total cross section of TI is comparable with DC2 and SC3. Note that SC1 is much weaker than DC1 and even weaker than SC2. The electrons preferably move together, which indicates for the importance of electron correlation and symmetries for this collision system.

Within the MO model the final state of SC1 at infinite internuclear distance can be reached by the two molecular

states $X\,^1\Sigma_g$ and $b\,^3\Sigma_u$. At all internuclear distances the molecular ground state $X\,^1\Sigma_g$ is well separated in energy from all initially populated states. Because the strength of the dynamical couplings between two states scales antiproportional with the energy gap, the dynamical population of $X\,^1\Sigma_g$ is weak (correlation diagrams can be found in [1,44–47]). Otherwise $b\,^3\Sigma_u$ as well as one of the initially populated states converges to the same binding energy at the limit of united atoms and $b\,^3\Sigma_u$ connects $He^{2+}+He(1s^2)$ and $He^+(1s)+He^+(1s)$ in energy space. But as a consequence of spatial and fermionic symmetry of the system the $b\,^3\Sigma_u$ is a spin triplet and therefore cannot be populated by any dynamical coupling. Thus the weakness of SC1 is a direct consequence of the electron entanglement caused by the symmetry of the system.

B. Single differential cross sections

Considering the conservation laws and the rotational symmetry of the problem around the beam axis, the three particles in the final state of TI and SI are completely characterized by four linearly independent quantities and the discrete values of the final state binding energy. We choose the momentum of the recoil ion perpendicular to the beam axis $p_{\perp,rec}$ and the three-dimensional momentum vector $\mathbf{p}'_e$ of the electron in a coordinate system, which is defined by the beam direction (z axis) and the recoil momentum vector $\mathbf{p}_{rec}$ for the presentation of our data.

The electron momentum perpendicular to the beam axis $p_{\perp,e}$ was found to be much smaller than $p_{\perp,rec}$ (see Fig. 2). Therefore the transverse momenta of the recoil ion $p_{\perp,rec}$ and the scattered projectile compensate each other. Within a semiclassical description $p_{\perp,rec}$ is a direct measure of the impact parameter. Figure 3 shows the single differential cross section $d\sigma/p_{\perp,rec}$ for four projectile velocities v_p. Distant collisions (very small $p_{\perp,rec}$) lead mainly to SI1. By increasing momentum transfer the ratio between SI1 and TI1 is oscillating around 1.

Similar oscillations can be observed at pure electron transfer reactions and can be understood within the MO description [1,45]. They are known to appear even at relatively large velocities, where the MO description is expected to be problematic [48]. In a single electron MO basis a ground state electron localized at one nucleus is described by a linear combination of the $1s\sigma_g$ and the $2p\sigma_u$ state. For the double electron capture it was shown that the oscillating structure of the differential cross section is related to the Σ_g, Σ_u interference [2,1]. The phase difference between $1s\sigma_g$ and $2p\sigma_u$ determines the positioning of the electron either at the recoil ion or the projectile and constitutes the difference between TI and SI. The strength of the oscillations indicates that the amplitude for these two MOs are comparable.

For electron emission with simultaneous excitation of the second electron the character of the single differential cross sections is completely different. At the smallest projectile velocity ($v_p=0.71$ a.u.) $d\sigma/p_{\perp,rec}$ of SI2 and TI2 is identical within the experimental error. This indicates that only states with one symmetry contribute to the population of the $He^+(2l)$ final state.
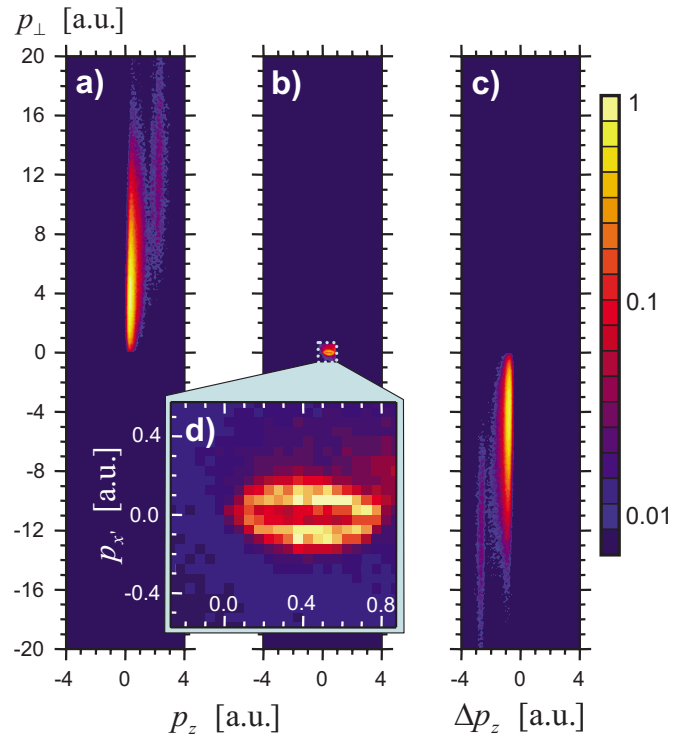

FIG. 2. (Color online) Transfer ionization at $v_p=0.86$ a.u. Momentum distribution of (a) the recoil ion and (b) the electron in the laboratory system (projectile moves from left to right along z). (c) Momentum change of the projectile. (d) Expanded electron distribution projected onto the nuclear scattering plane ($x',z'=z$) on linear color scale.

To the best of our knowledge TI2 and SI2 are theoretically not described in the literature. It can be expected, that at small internuclear distances TI2 and SI2 proceed similar to the two-electron excitation,

$$He^{2+} + He \rightarrow He^{2+} + He(2l,2l) \tag{3}$$
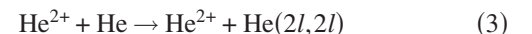
which has been investigated theoretically by Koike *et al.* [49]. They investigated a MO promotion, which is initialized by the radial coupling between the $^1\Sigma_g^+(2s\sigma_u^2)$ and $^1\Sigma_g^+(2p\sigma_u^2)$ state. This coupling occurs at a hidden crossing of these two states at an internuclear distance of about 0.2 a.u. [50]. Considering a screened nuclear charge of 1 a.u. a classical Coulomb scattering with an impact parameter of 0.2 a.u. would lead to the momentum exchange, which is marked by arrows at Fig. 3. The experimental $d\sigma/p_{\perp,rec}$ of TI2 and SI2 strongly decrease left of the arrows, while the Rutherford cross section would show a $p_{\perp,rec}^{-3}$ dependence. Therefore we conclude that the MO promotion of TI2 and SI2 has to pass through the same hidden crossing, which initializes the two electron excitation.

The autoionizing double capture (ADC), which is a two step process, is another channel closely related to TI2, SI2, and the two-electron excitation. ADC starts with a double electron capture into doubly excited states of the projectile. In a second step the $He^*(2l,2l)$ projectile autoionizes,

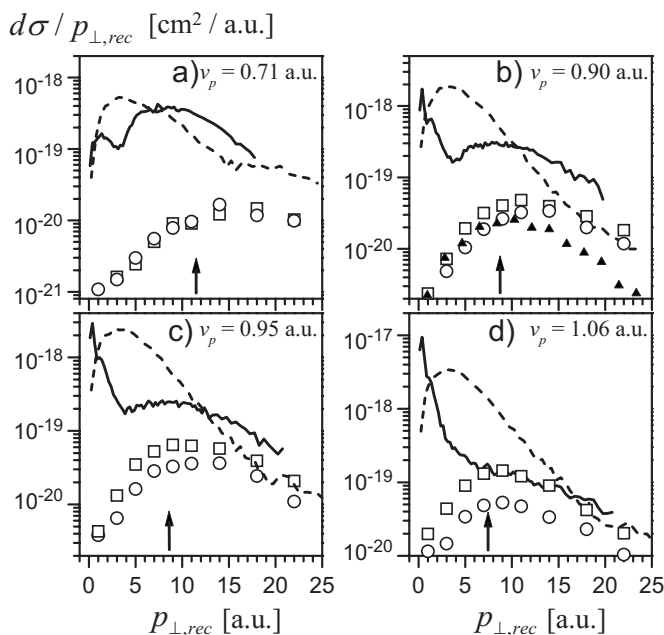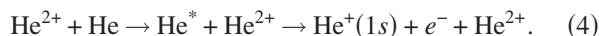FIG. 3. Recoil-ion transverse momentum distributions for electron emission in He^{2+}+He collisions at four projectile velocities v_p between 0.71 and 1.06 a.u.: SI1 (solid lines), SI2 (circles), TI1 (dashed lines), and TI2 (squares). Total cross sections are normalized to [42]. Autoionizing double capture for v_p=0.90 a.u. scaled by an arbitrary factor (triangles).

$$He^{2+} + He \rightarrow He^{*} + He^{2+} \rightarrow He^{+}(1s) + e^{-} + He^{2+}. \quad (4)$$

The lifetime of He* is less than 1 ns and therefore the ADC is a particular two step mechanism which contributes to TI1 signal. The binding energy difference between He* and He$^{+}(1s)$ is about 35 eV. Therefore the electrons produced by the ADC are emitted from the projectile system with a fixed momentum of about 1.6 a.u. Even though the ADC is only a very weak contribution to TI1 it can be separated by the electron momentum distribution shown in Fig. 4. While the spectrometer was optimized for electrons with small momenta at the laboratory frame and projectile frame, the ADC had only been detected within a small solid angel. For v_p =0.9 a.u. the single differential cross section $d\sigma/p_{\perp,rec}$ of electrons emitted with the signature of ADC into the acceptance angle of the spectrometer is shown at Fig. 3(b). The similar shape of TI2, SI2, and ADC is another indication, that at small internuclear distances these channels pass through the same MO promotion.

C. Electron emission pattern

The single differential cross sections discussed in the previous section could be qualitatively understood in the MO picture. We now show that the characteristics of the lowest MOs in the electron promotion to the continuum can be retrieved from the electron emission pattern.

For the presentation we choose a coordinate system (x',y',z'), which is defined individually for each event by the nuclear motion. The x' axis is given by the direction of $p_{\perp,rec}$ and the z' axis ($=z$ axis) is the projectile beam axis.
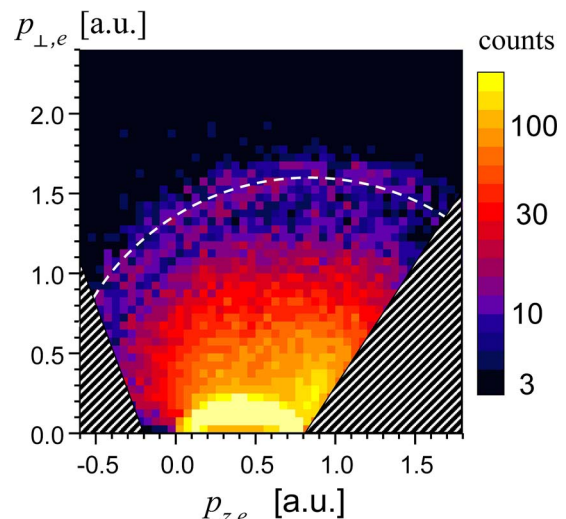

FIG. 4. (Color online) Electron momentum distribution of TI1 at v_p=0.84 a.u. The z axis is defined by the incoming beam direction and $p_{r,e}$ is the radial component of the electron momentum. The circular arc marks the position where electrons emitted with 35 eV from the projectile are found. The hatched area was not detected.

The nuclear scattering plane is defined by x',z' and the y' axis is the normal to this plane. While in the laboratory frame the electron momentum distribution is rotational symmetric, there is only a mirror symmetry with respect to the scattering plane (x',z') in the internal coordinates. Projections of the electron distribution onto the scattering plane have been termed "top view" in the literature [17]. Figure 5 shows top view distributions of TI1. The electron velocities are normalized to the projectile velocity. The projectile nucleus is found at $(1,0)$ and the target nucleus at $(0,0)$. By the nuclear momentum exchange during the collision the target is shifted an indiscernible small value upward and the projectile downward.

The normalization of the electron velocities causes a similar size of the top view distributions for all different projectile velocities v_p. This scaled presentation makes obvious, that the key determinant for the electron emission pattern at these velocities is the position of the two nuclei in velocity space. This is completely different from the situation in fast collisions (see, e.g., [51–55] for similar plots for fast collisions). The experiments done in the late 1980s [7–10] tried to identify a sharp maximum of the electron distribution at the saddle point to support the classical saddle point model. Our data in Fig. 5 make it obvious why they had to fail.

Contradictory to the most simple version of the saddle point model, we find a local minimum for electrons emitted with small transversal velocities. Therefore the probability to find electrons exactly with the velocity of the saddle point is much smaller than for many other velocities. While the early experiments in Rolla [9,10] and Bariloche measured the electron velocity distribution only under a certain angles to the beam axis, they had not been able to discover the structure of the electron emission pattern. Our data show that the velocity distribution in the laboratory frame strongly depends on this angle and this might be an explanation for the disagreement between these publications.
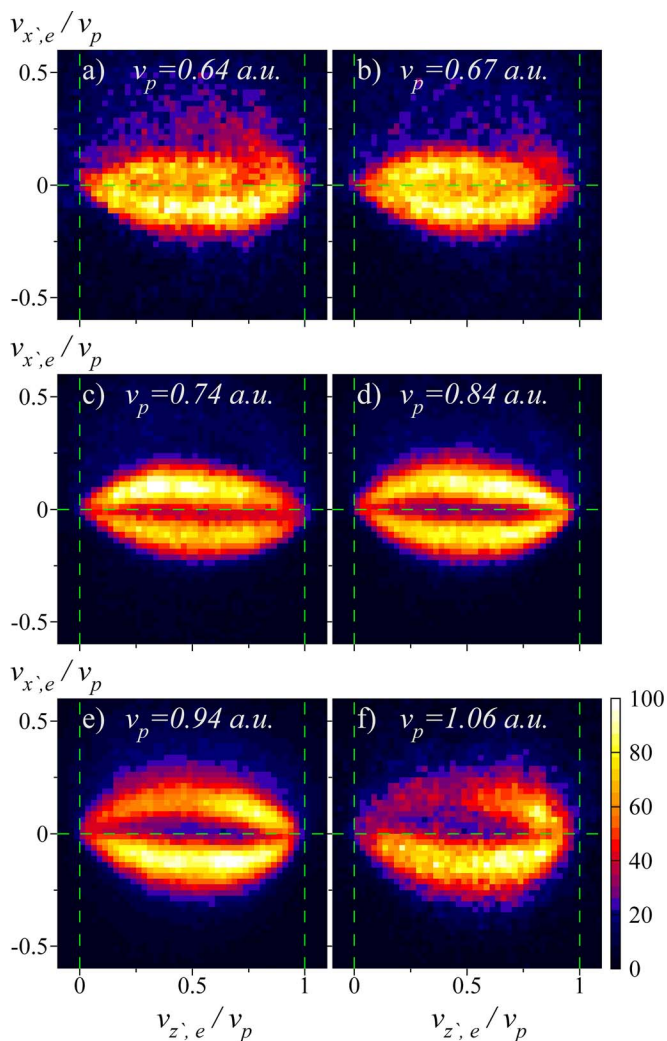
FIG. 5. (Color online) "Top view" of the electron distribution for TI1 at six projectile velocities v_p between 0.64 a.u. and 1.06 a.u. The normalized electron velocities are projected onto the plane of nuclear motion (projectile motion from left to right). At the initial state the projectile is located at (1,0) and the target at (0,0). During the reaction the projectile is scattered downwards and the target upwards.

While hand waving classical arguments cannot explain this minimum, the consideration of the symmetries of the involved MOs is sufficient for a qualitative understanding of this structure [56]. The electronic Hamiltonian of a molecule is rotational symmetric to the internuclear axis. Therefore a factor $\exp(im\phi)$ can be separated from all molecular eigenstates, where the azimuthal angle ϕ describes the rotation around this symmetry axis and the quantum number m (related to the magnetic quantum number in an atom) is an integer. The initial state, where all electrons are in the spherical symmetrical $He(1s^2)$, is exclusively composed by MOs with $m=0$ (σ states). As the two nuclei pass each other, the rotation of the molecular axis results in the population of further MOs, especially those with $m\pm1$ (π states). Because the system is symmetric to the plane of nuclear motion during the whole process, only π states orientated in the scattering plane can be populated. Their angular momentum is
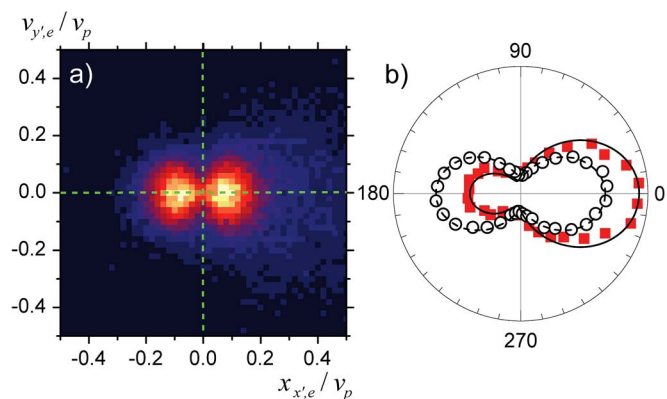

FIG. 6. (Color online) TI at $v_p=0.84$ a.u.: Electron velocity distribution in the x',y' plane (i.e., normal to the projectile beam axis) for $0.3v_p<v_{z,e}<0.7v_p$. (a) Density plot of $d^2\sigma/(dv_{x',e}dv_{y',e})$. The recoil ion is scattered to the right side. (b) Polar presentation of $d^2\sigma/(d\phi dv_{r,e})$ for $v_{r,e}=\sqrt{v_{x',e}^2+v_{y',e}^2}=0.2v_p$ (circles) and $v_{r,e}=0.4v_p$ (squares). For $v_{r,e}=0.2v_p$, the measured data can be described by $d^2\sigma/(d\phi dv_{r,e})\propto 0.66\cos^2\phi+0.33$ (dashed line) and for $v_{r,e}=0.4v_p$ with $d^2\sigma/(d\phi dv_{r,e})\propto 0.66\cos^2\phi+0.66\cos\phi+0.33$ (solid line).

provided by the nuclear motion, thus the angular momentum has to be perpendicular to the scattering plane. These states have a $\cos\phi$ dependency with $\phi=0$ directed to $p_{\perp,rec}$.

In the final state the internuclear axis has turned into the beam direction (z' axis). Since the signature of σ and π states appear in the plane perpendicular to this axis, projection of the electron distribution onto the x', y' plane is promising to investigate the rotational couplings.

As an example of such a presentation, Fig. 6(a) shows the TI1 at $v_p=0.84$ a.u. In Fig. 6(b) the corresponding polar plots of the double differential cross section $d^2\sigma/(d\phi\,dv_{r,e})$ are presented at two different electron transversal velocities $v_{r,e}=\sqrt{v_{x',e}^2+v_{y',e}^2}$. At $v_{r,e}=0.2\,v_p$ (circles) the experimental results can be approximated by a $\cos^2\phi$ distribution, the emission characteristic of molecular π states. The solid curve, which fits well to the data, is a sum of a $\cos^2$ and an isotropic contribution originating from a σ state. While at small $v_{r,e}$ the data in Fig. 5(b) show a left-right symmetry, as expected for a pure σ or π state, this symmetry breaks down at larger $v_{r,e}$ [squares in Fig. 6(b)]. To shift the contribution to the recoil side ($v_{x',e}>0$), a $\cos\phi$ term has to be added to the fit [dashed line at Fig. 6(b)]. This additional term originates from interferences between σ and π states and its strength depends on the relative phase between these contributions.

We now turn to the influence of the second, bound electron on the continuum electron momentum distributions. Figure 7 shows the top view presentations at $v_p=0.9$ a.u. of all four distinguishable channels. In the upper two spectra, the bound electron is in the ground state, either of the projectile [Fig. 7(a)] or at the target [Fig. 7(b)]. The local minimum at $v_{x',e}=0$, which was observed at TI1 for all projectile velocities is not present for SI1. This indicates the major part of the SI1 promotion occurs without rotational coupling. The ionization dynamics for the two channels is hence completely different.
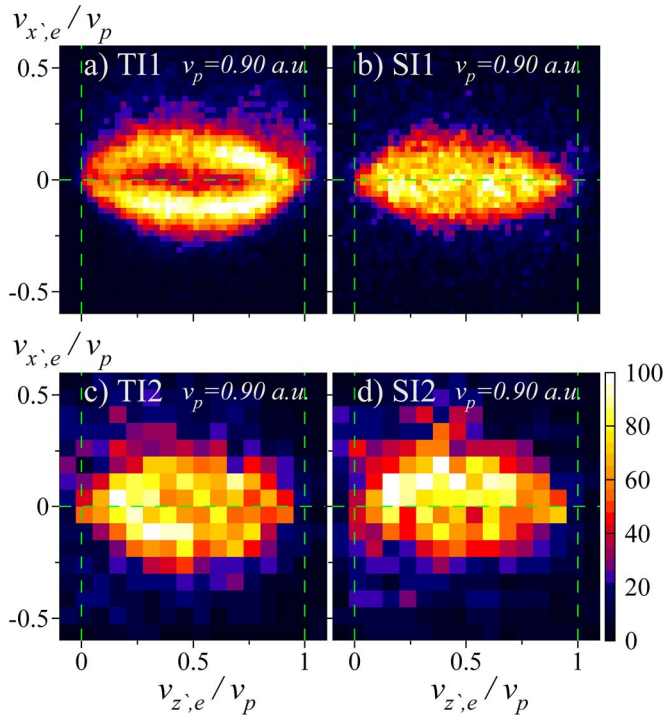
FIG. 7. (Color online) Top view as Fig. 4 (projection of the electron velocity distribution onto the scattering plane) but (a) TI1, (b) SI1, (c) TI2, and (d) SI2 at v_p=0.9 a.u.

The cross sections of the two channels, where the bound electron is in an excited state [Figs. 7(c) and 7(d)], are more than one order of magnitude smaller than those of TI1 and SI1. Both of these spectra show a slightly higher probability to find the emitted electron closer to the target nucleus than to the projectile.

To better visualize a σ or π character also for the weak channels with small statistics Fig. 8 shows the electron distribution in direction of the nuclear momentum exchange (x' axis) for a slice with 0.3 a.u. $<v_{z',e}<0.7$ a.u. A local minimum at $v_{x',e}$=0 is visible for TI2 and SI2 as well as TI1, whereas SI1 [Fig. 8(b), solid line] shows a maximum.

Are these striking differences of the momentum distribution for different final states of the second electron caused by electron correlation? In an independent electron model, the electron emission pattern would be independent of the final state of the bound electron. We will show now that, nevertheless the electron-electron repulsion is not the reason for the differences.

The three-dimensional electron distribution discussed so far does not represent a fully differential cross section because the momentum exchange $p_{\perp,rec}$ is not fixed, but integrated over. Figure 3 shows that the relevant impact parameters for the different channels are very different. While the dominant contribution to SI1 arises from distant collisions, the other channels require close collisions. One might expect that the differences in the electron emission pattern are primarily related to the different contributions of nuclear trajectories.

To test this assumption, we split the one-dimensional electron distribution of SI1 into a contribution of small nuclear
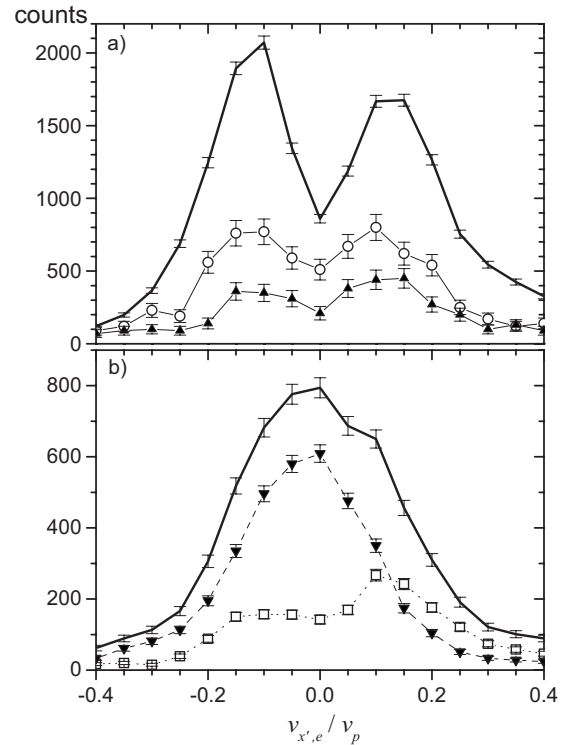

FIG. 8. $v_{x',e}$ distribution at v_p=0.9 a.u. for electrons with $-0.2v_p<v_{z',e}<0.2v_p$. (a) TI1 (line), TI2 (open circles), and SI2 (full triangles). (b) Total SI1 (line) and events with $p_{r,rec}<5$ a.u. (full inverted triangles) and with $p_{r,rec}>7$ a.u. (open squares).

momentum exchange, e.g., distant collisions [triangles at Fig. 8(b)] and close collisions [squares at Fig. 8(b)]. The corresponding top view presentations are shown in Fig. 9. By selecting small momentum exchange at SI1, the electrons become even more concentrated at $v_{x',e}$=0, which is the signature of a σ states dominated promotion. The π state contribution to SI1 is visible at the small contribution from close collisions. From these figures we conclude that the difference in electron emission pattern of the four channels mainly results from the impact parameter dependence of the channels.

This does not mean that electron correlation is unimportant for the process. Because the structure of the He$_2^{2+}$ correlation diagram cannot be understood as a combination of

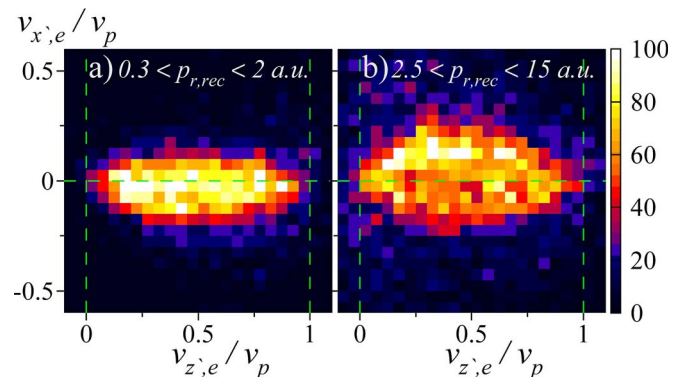FIG. 9. (Color online) Top view of SI1 at v_p=0.9 a.u.: (a) distant collisions with 0.3 a.u.$<p_{r,rec}<2$ a.u., (b) close collisions with 2.5 a.u.$<p_{r,rec}<15$ a.u.

two single electron correlation diagrams the impact parameter dependence cannot be described without taking electron correlation into account. Electron correlation in terms of many particle symmetries is essential for the understanding of MO promotion.

IV. SUMMARY

We have investigated the electron emission from He_2^{2+} quasimolecules produced at slow He^{2+}+He collisions. The kinematically complete measurement distinguishes four reaction channels of different final states of the bound electron.

Prominent positions in the electron emission pattern have been found at the positions of the two nuclei in velocity space. In contrast to the classical saddle point model most of the reaction channels show a local minimum of the electron velocity distribution at the saddle point of the nuclear potential, which is exactly located between the two nuclei in case of equal nuclear charge.

We have shown that the description of the reaction dynamic as a molecular orbital (MO) promotion provides a qualitatively good understanding of the recoil transversal momentum differential cross section $d\sigma/p_{\perp,rec}$. Our experimental three-dimensional electron momentum distributions show the symmetry of bound σ or π orbitals, depending on the impact parameter and reaction channel. The data strongly suggest that the symmetry of the initially populated MOs is preserved upon promotion of the electron to the continuum. The relevance of rotational coupling during the MO promotion can be seen already in the single differential cross section $d\sigma/p_{\perp,rec}$ and it also is reflected in the electron emission pattern. The observed strong dependence of the electron emission pattern as well as the nuclear momentum exchange on the reaction channel can be ascribed to the same cause, namely the necessity of specific couplings at the related MO promotion. A satisfactory theoretical treatment of even such a simple and fundamental collision system as He^{2+} on He containing two active electrons is still missing.

[1] V. López, A. Macías, R. D. Piacentini, A. Riera, and M. Yánez, J. Phys. B **11**, 2889 (1978).

[2] R. S. Gao, C. M. Dutta, N. F. Lane, K. A. Smith, R. F. Stebbings, and M. Kimura, Phys. Rev. A **45**, 6388 (1992).

[3] R. E. Olson, Phys. Rev. A **33**, 4397 (1986).

[4] R. E. Olson, T. J. Gay, H. G. Berry, E. B. Hale, and V. D. Irby, Phys. Rev. Lett. **59**, 36 (1987).

[5] R. E. Olson, C. R. Feeler, C. J. Wood, C. L. Cocke, R. Dörner, V. Mergel, H. Schmidt-Böcking, and J. Ullrich, Nucl. Instrum. Methods Phys. Res. B **124**, 249 (1997).

[6] R. E. Olson, Phys. Rev. A **27**, 1871 (1983).

[7] V. D. Irby, T. J. Gay, J. Wm. Edwards, E. B. Hale, M. L. McKenzie, and R. E. Olson, Phys. Rev. A **37**, 3612 (1988).

[8] T. J. Gay, M. W. Gealy, and M. E. Rudd, J. Phys. B **23**, L823 (1990).

[9] G. C. Bernardi, S. Suárez, P. D. Fainstein, C. R. Garibotti, W. Meckbach, and P. Focke, Phys. Rev. A **40**, 6863 (1989).

[10] G. Bernardi, P. Fainstein, C. R. Garibotti, and S. Suarez, J. Phys. B **23**, L139 (1990).

[11] W. Meckbach, S. Suarez, P. Focke, and G. Bernardi, J. Phys. B **24**, 3763 (1991).

[12] M. Pieksma, S. Y. Ovchinnikov, J. van Eck, W. B. Westerveld, and A. Niehaus, Phys. Rev. Lett. **73**, 46 (1994).

[13] S. D. Kravis, M. Abdallah, C. L. Cocke, C. D. Lin, M. Stockli, B. Walch, Y. D. Wang, R. E. Olson, V. D. Rodríguez, W. Wu, M. Pieksma, and N. Watanabe, Phys. Rev. A **54**, 1394 (1996).

[14] R. Dörner, H. Khemliche, M. H. Prior, C. L. Cocke, J. A. Gary, R. E. Olson, V. Mergel, J. Ullrich, and H. Schmidt-Böcking, Phys. Rev. Lett. **77**, 4520 (1996).

[15] M. Abdallah, S. Kravis, C. L. Cocke, Y. Wang, V. D. Rodriguez, and M. Stöckli, Phys. Rev. A **56**, 2000 (1997).

[16] M. A. Abdallah, C. L. Cocke, W. Wolff, H. Wolf, S. D. Kravis, M. Stöckli, and E. Kamber, Phys. Rev. Lett. **81**, 3627 (1998).

[17] M. A. Abdallah, W. Wolff, H. E. Wolf, C. L. Cocke, and M. Stöckli, Phys. Rev. A **58**, R3379 (1998).

[18] M. A. Abdallah, W. Wolff, H. E. Wolf, C. L. Cocke, and M. Stöckli, J. Phys. B **32**, 4237 (1999).

[19] M. Abdallah, S. Kravis, C. L. Cocke, Y. D. Wang, M. Stockli, and R. E. Olson, Phys. Scr., T **73**, 219 (1997).

[20] E. Edgü-Fry, C. L. Cocke, E. Sidky, C. D. Lin, and M. Abdallah, J. Phys. B **35**, 2603 (2002).

[21] F. Afaneh, R. Dörner, L. Schmidt, Th. Weber, K. E. Stiebing, O. Jagutzki, and H. Schmidt-Böcking, J. Phys. B **35**, L229 (2002).

[22] L. Ph. H. Schmidt, F. Afaneh, M. Schöffler, J. Titze, O. Jagutzki, Th. Weber, K. E. Stiebing, R. Dörner, and H. Schmidt-Böcking, Phys. Scr., T **110**, 379 (2004).

[23] Emil Y. Sidky, Clara Illescas, and C. D. Lin, Phys. Rev. Lett. **85**, 1634 (2000).

[24] C. Illescas, I. Rabadán, and A. Riera, Phys. Rev. A **57**, 1809 (1998).

[25] G. Bandarage and R. Parson, Phys. Rev. A **41**, 5878 (1990).

[26] J. H. Macek, S. Yu. Ovchinnikov, and S. V. Pasovets, Phys. Rev. Lett. **74**, 4631 (1995).

[27] E. A. Solov'ev, Sov. Phys. JETP **63**, 678 (1986).

[28] M. Pieksma and S. Yu. Ovchinnikov, J. Phys. B **24**, 2699 (1991).

[29] Emil Y. Sidky and C. D. Lin, Phys. Rev. A **60**, 377 (1999).

[30] Emil Y. Sidky and C. D. Lin, J. Phys. B **31**, 2949 (1998).

[31] M. Chassid and M. Horbatsch, Phys. Rev. A **66**, 012714 (2002).

[32] D. R. Schultz, C. O. Reinhold, P. S. Krstić, and M. R. Strayer, Phys. Rev. A **65**, 052722 (2002).

[33] S. Yu. Ovchinnikov and J. H. Macek, Phys. Rev. Lett. **75**, 2474 (1995).

[34] L. Schmidt, Ph.D. thesis, Johann-Wolfgang-Goethe Universität

Frankfurt, 2000.

[35] J. Ullrich, R. Moshammer, A. Dorn, R. Dörner, L. Ph. H. Schmidt, and H. Schmidt-Böcking, Rep. Prog. Phys. **66**, 1463 (2003).

[36] R. Dörner, V. Mergel, O. Jagutzki, L. Spielberger, J. Ullrich, R. Moshammer, and H. Schmidt-Böcking, Phys. Rep. **330**, 95 (2000).

[37] R. Dörner *et al.*, Nucl. Instrum. Methods Phys. Res. B **124**, 225 (1997).

[38] O. Jagutzki, V. Mergel, K. Ullmann-Pfleger, L. Spielberger, U. Spillmann, R. Dörner, and H. Schmidt-Böcking, Nucl. Instrum. Methods Phys. Res. A **477**, 244 (2002).

[39] V. Mergel, Ph.D. thesis, Universität Frankfurt, Shaker, Aachen, 1996.

[40] R. Dörner *et al.*, Phys. Rev. A **57**, 1074 (1998).

[41] W. C. Wiley and I. H. McLaren, Rev. Sci. Instrum. **26**, 1150 (1955).

[42] V. V. Afrosimov, G. A. Leiko, Yu. A. Mamaev, and M. N. Panov, Sov. Phys. JETP **40**, 661 (1975).

[43] R. D. DuBois, Phys. Rev. A **36**, 2585 (1987).

[44] W. J. Fritsch, J. Phys. B **27**, 3461 (1994).

[45] C. Harel and A. Salin, J. Phys. B **13**, 785 (1980).

[46] H. Yagisawa, H. Sato, and T. Watanabe, Phys. Rev. A **16**, 1352 (1977).

[47] S. Hara and H. Sato, J. Phys. B **11**, 955 (1978).

[48] V. Mergel *et al.*, Nucl. Instrum. Methods Phys. Res. B **98**, 593 (1995).

[49] F. Koike, H. Nakamura, S. Hara, Y. Itikawai, M. Matsuzawac, H. Sato, and I. Shimamural, J. Phys. B **11**, 4193 (1978).

[50] S. Hara and H. Sato, J. Phys. B **11**, 4193 (1978).

[51] C. J. Wood, R. E. Olson, W. Schmitt, R. Moshammer, and J. Ullrich, Phys. Rev. A **56**, 3746 (1997).

[52] R. Moshammer, J. Ullrich, H. Kollmus, W. Schmitt, M. Unverzagt, H. Schmidt-Böcking, C. J. Wood, and R. E. Olson, Phys. Rev. A **56**, 1351 (1997).

[53] R. Moshammer *et al.*, Phys. Rev. Lett. **73**, 3371 (1994).

[54] M. Schulz, R. Moshammer, D. Fischer, and J. Ullrich, J. Phys. B **37**, 4055 (2004).

[55] Th. Weber *et al.*, J. Phys. B **33**, 3331 (2000).

[56] M. Pieksma and S. Yu. Ovchinnikov, J. Phys. B **27**, 4573 (1994).